 doi:10.20944/preprints202105.0542.v1

Article

Development and analysis of the novel hybridization of a single flash geothermal power plant with biomass driven sCO2-steam Rankine combined cycle

Balkan Mutlu [1,2]*, Derek Baker [1,2] and Feyza Kazanç [1]

[1] Department of Mechanical Engineering, Middle East Technical University, Ankara 06800, Turkey;
[2] Center for Solar Energy Research and Applications (GÜNAM), Ankara 06800, Turkey;
* Correspondence: balkanmutlu@gmail.com;

Abstract: This study investigates the hybridization scenario of a single flash geothermal power plant with a biomass driven sCO2-steam Rankine combined cycle where a solid local biomass source, olive residue, is used as a fuel. The hybrid power plant is modeled using the simulation software EBSILON®Professional. A topping sCO2 cycle is specifically chosen for its potential for flexible electricity generation. A synergy between the topping sCO2 and bottoming steam Rankine cycles is achieved by a good temperature match between the coupling heat exchanger where the waste heat from the topping cycle is utilized in the bottoming cycle. The high temperature heat addition problem common sCO2 cycles is also eliminated by utilizing the heat in the flue gas in the bottoming cycle. Combined cycle thermal efficiency and biomass to electricity conversion efficiency of 24.9% and 22.4% are achieved, respectively. The corresponding fuel consumption of the hybridized plant is found as 2.2 kg/s.

Keywords: hybridization, single-flash, geothermal, biomass, sCO2 cycle, olive residue, flexibility

1. Introduction

The performance of geothermal power plants can degrade over years as the geothermal resource is exploited. This degradation can be due to decreases in fluid temperature, flow rate, and pressure at the production wellhead over the lifetime of the geothermal resource. These decreases can reduce both the quantity (thermal energy) and quality (temperature) of the heat input, and lead to reductions in both the output and the thermal efficiency of the plant [1]. The performance of geothermal power plants is also typically affected negatively by increases in ambient temperatures, especially during hot summer months. The power fluctuations due to the changes in ambient temperatures can exceed 20% in some scenarios [2]. The hybridization of geothermal resources with other renewable thermal energy resources offers the potential to increase the performance of geothermal power plants while being economically feasible since the need for land and grid infrastructure can be reduced or eliminated. However, hybridization of geothermal energy with other renewable thermal energy resources becomes a site-specific matter due to the site-specific nature of the geothermal energy itself [3]. In the context of this article, Kızıldere-1 (KZD-1), an existing single flash Geothermal Electric Power Plant (GEPP) operating significantly below design capacity, is considered as a case study for hybridization with biomass energy. KZD-1 is located on the Western Anatolia region of Turkey where Olive Residue (OR) exists as an abundant solid biomass resource. The hybridization scenario in this article concentrates on bringing the underutilized KZD-1 GEPP to its full capacity by the use of thermal heat derived from this local biomass source. Colocation of geothermal and biomass as secondary renewable thermal energy source is exploited through utilizing the unused capacity of KZD-1 turbine and introducing a next generation

power cycle, i.e., supercritical CO_2 (sCO2) cycle, as a topping cycle. A sCO2 cycle is specifically chosen for its potential to support flexible electricity generation. The article is structured to allow the method and outcomes to be adapted to other GEPP.

The interest in hybridization of geothermal with biomass is limited in the literature. The state-of-the-art studies are limited to those using biomass sourced heat to supplement the operating enthalpy of low temperature geothermal [4], using biomass to compensate for the off-design conditions of a geothermal power plant [5], and multigeneration biogas-geothermal systems [6]. When the colocation of geothermal and agricultural lands or forestry are present, either biomass or geothermal is used to boost the performance of the other for actual industrial applications. For instance, a dry steam geothermal power plant in Cordia, Italy, operating below its rated output of 20 MWe is redesigned to accommodate a biomass furnace in order to superheat the geothermal steam. An additional 5.4 MWe gain is obtained from the biomass combustion. In another example, a wood waste biomass power plant operating in close proximity to forest plantations in New Zealand is supplemented by a geothermal preheat [7].

Despite the limited studies on hybridization of geothermal with biomass, literature on hybridization of flash type geothermal power plants with solar thermal is more developed [8] and can provide input to the design of hybrid geothermal-biomass power plants. Solar thermal heat is used in most of these studies either to preheat or superheat the geothermal working fluid. Initial efforts on hybrid solar-geothermal power plant models are by Lentz and Almanza [9,10] where a Direct Steam Generation (DSG) solar field is theoretically coupled to two different locations of the Cerro Prieto geothermal single flash plant in Mexico. In both of their proposed models, geothermal brine is allowed to pass through the tubes of a Parabolic Trough Collector (PTC) field with the purpose of increasing the flow rate of geothermal steam 10%. Mir et al. [11] developed a thermodynamic model to estimate the production of a hypothetical solar-geothermal power plant in Northern Chile for two different operational modes: 1) Peak Power mode with constant geothermal output where the solar input increases the power output; and 2) Save Geothermal Resource mode with constant power output and the use of geothermal resources decreases with increases in solar input. Note that although individual authors often used different names for these modes, this naming is used for clarity and consistency within this section. Mir et al. [11] added solar heat to a single flash geothermal power plant from a PTC field to produce superheated steam and additional saturated steam from the separator whenever possible. With the assistance of the solar heat, up to 11.6% increase in energy production from the geothermal brine is obtained for the Peak Power mode, whereas savings up to 10.3% in the use of geothermal resources is obtained for the Save Geothermal Resource mode. Cardemil et al. [12] conducted energetic and exergetic analyses for hypothetical single and double flash geothermal power plants, each having four different brine characteristics, taking Save Geothermal Resource and Peak Power modes into account. A PTC field is used to supply solar heat to the system after the separator, both to the geothermal brine and as additional steam and superheat, respectively. Their results show that a hybrid single flash power plant can produce at least 20% additional power output depending on the brine characteristics. For all of the analyzed cases, at least 3% increase is observed for first law efficiencies. For the Save Geothermal Resource mode where the plant power output stays constant when solar resources are available, 16% and 19% reductions in geothermal fluid consumption are observed for flash and double flash configurations, respectively. A more recent and comprehensive study on hybridization of flash type geothermal power plants is conducted by McTigue et al. [13]. In their study, an existing double flash power plant operating in China Lake, California, is hybridized with solar thermal to increase the power generation. It is aimed to increase the power output of the geothermal turbine operating at 75% of its rated output (22.5 MW) to 100% of its rated output (30 MW) by integrating an array of PTCs. In order to decide the optimum point for solar thermal heat addition from the PTC heat transfer fluid to the double flash geothermal power plant, parametric analyses on thermal efficiency are compared for 4

different points within the double flash GEPP. The optimum point for heat addition is found as the brine after the first flash tank separator. The solar heat added to this brine is converted to electricity with an efficiency of 24.3%. Alternate thermal storage scenarios are also investigated for dispatchable electricity generation. Overall, Levelized Cost of Electricity (LCOE) with 3 hours of thermal energy storage is calculated as 0.08 $/kWhe, which is lower than equivalent conventional standalone CSP and battery integrated PV systems. It is concluded that hybridization can be cost effective since the existing power block, pipework, and condenser are shared.

A novel hybrid solar integration for a binary type geothermal plant is proposed by Bonyadi et al. [14]. Although binary plants have different characteristics than the flash type plants, their introduction of a topping cycle for hybridization formed an inspiration for the efforts in this article. Bonyadi et al. [14] added a solar powered steam Rankine topping cycle to a hypothetical binary geothermal power plant without requiring any physical modification or deviation from design conditions of the bottoming Organic Rankine Cycle (ORC). The solar topping cycle is coupled to the ORC such that the waste heat from the topping cycle is utilized in the ORC. Their representative design has an incremental solar efficiency of 12.2% for Peak Power mode and consumes up to 17% less brine than a similar stand-alone geothermal plant for Save Geothermal Resource mode.

For the completely different technology of Enhanced Geothermal System (EGS), Jiang et al. [15] integrated solar thermal heat into a hypothetical EGS where CO_2 is used as both heat transmission fluid for geothermal and working fluid for the sCO2 power cycle. Their hybrid system uses geothermal energy as the primary energy source to provide the base-load electricity and the solar energy is used as a supplement to meet the peak demand whenever possible. Their hybrid plant reaches the maximum thermal efficiency of 22.44% for a CO_2 turbine inlet temperature of 600 °C.

The sCO2 cycle studied in this article is a part-flow type sCO2 cycle. Despite the equivalent or higher thermodynamical efficiencies of sCO2 cycles compared to their steam Rankine counterparts, there has not been a full-scale commercial demonstration for sCO2 cycles as the studies are limited to laboratory-scale test setups under 1 MW [16–19]. The underlying reason for sCO2 cycles offering good thermal efficiencies is that compression work of CO_2 as a working fluid close to its critical point of 31.1°C and 7.39 MPa is minimal [20]. However, thermophysical properties of CO_2 such as the isobaric heat capacity in the vicinity of its critical point exhibit non-linear behavior, and result in a pinch point problem. Utamura [21] demonstrated that a first law efficiency of 45% under maximum operating conditions of 20 MPa and 526.9 °C is achievable for part-flow sCO2 cycles where the pinch point problem can be avoided. The part-flow configuration helps to confine the likelihood of pinch point problems to the low temperature recuperator (LTR) owing to splitting the rest of the recuperation process to a high temperature recuperator (HTR). Overall, part-flow sCO2 cycles can offer more than 5% increase in the thermal efficiency compared to simple recuperated sCO2 cycles and are the most extensively researched sCO2 cycle in the literature due to being relatively simple while retaining good efficiencies [22]. In addition to the pinch-point problem, the sCO2 cycles have another intrinsic problem regarding the heat addition to the cycle. Due to their highly recuperative characteristics, the external heat addition to sCO2 cycles is done over a high temperature interval [23–25]. In order to overcome this limitation, the sCO2 cycles are often combined with bottoming ORC cycles operating at low temperatures [26–29], or utilized in cascaded manner as sCO2-sCO2 and sCO2-transcritical carbon dioxide (tCO2) cycles [23–25]. Alternatively, for coal powered sCO2 cycle designs, advanced boiler and heater designs are introduced to fully exploit the heat available in the flue gas within the cycle at the cost of having more complex layouts [30,31]. Motivated by the problem of a biomass powered sCO2 cycle design, Manente and Lazzaretto [32] introduced a novel cascaded sCO2 cycle configuration using woody biomass as a fuel. In their study, two different cascaded sCO2 cycles, namely part flow-simple recuperated and simple recuperated-simple recuperated, are investigated along with four different biomass boiler arrangements. Their results showed that

part flow-simple recuperated cascaded sCO2 cycle design with a counter-current radiative-convective boiler demonstrates the best performance in terms of biomass to electricity conversion efficiency, i.e., either 34% or 36% depending on the presence of an air-preheating unit, for the topping cycle turbine inlet temperature (TIT) of 550 °C.

The work in this article aims to build-on this existing literature by presenting a novel scheme to hybridize an existing single flash GEPP with biomass derived heat that can be adapted to any site where colocation of these two renewable resource types is present. KZD-1 is used a case study to apply this novel method and analyze its performance.

2. Novel hybrid geothermal-biomass power plant scheme

Based on the reviewed literature, for an existing flash type GEPP suffering from a degradation in its geothermal resource in terms of decreased flow rate or enthalpy which ultimately causes reduced steam flow to its turbine, the following novel hybrid geothermal-biomass hybridization scheme can be adapted if colocated with a solid biomass resource. A part-flow sCO2 cycle to be operated at higher temperature than the existing geothermal cycle can be used as a topping cycle. The part-flow sCO2 cycle can reject its waste heat through its cooler to preheat the condensate of the existing geothermal cycle. A novel biomass heater-boiler designed for this unique application can supply high temperature heat from biomass combustion through radiative heat transfer to drive the part-flow sCO2 topping cycle and bring the preheated geothermal condensate to a certain steam quality. Medium temperature heat of the flue gas is transferred to this steam-water mixture by means of convective heat transfer to create dry steam. This 100% biomass energy derived dry steam can be fed to the steam turbine of an existing GEPP operating under capacity due to reduction in its mass flow. Moreover, when appropriate the existing unused cooling component capacity of GEPP can be used to condensate the biomass derived steam exhaust for better utilization. Such a novel hybridization scheme offers several advantages. First, the rejected heat of the topping sCO2 cycle is not lost, rather used to supply heat for additional dry steam. Second, sCO2 cycles are utilized either in cascaded manner [23–25,32] or combined with ORC bottoming cycles operating at low temperatures [26–29] due to their high temperature heat requirement. Since the medium temperature heat of the flue gas is used for creation of additional dry steam, the need of using an additional bottoming ORC or sCO2 cycle is eliminated. As a result, the existing GEPP can be brought to full capacity to allow better Capex utilization. Note that only the unused flow capacity of steam turbine, and if possible, existing cooling system is used for such a hybridization scenario while operational steam turbine inlet conditions, i.e., pressure and temperature, remain unchanged. In this sense, hybridization is possible without modifying the components of the existing GEPP.

2.1. Application of Proposed Novel Hybridization Scheme to KZD-1 GEPP

2.1.1. Existing conditions of KZD-1 GEPP

KZD-1 GEPP is the first geothermal power plant of Turkey commissioned in 1984 and currently operated by Zorlu Energy [33]. The steam mass flow rate feeding the steam turbine of KZD-1 decreased significantly over the years considering the differences between the current mass flow rate of 19.45 kg s^{-1} and the average steam mass flow rate of 33.34 kg s^{-1} reported by Gökçen et al. in 2004 [34]. Moreover, the steam turbine of KZD-1 seems to be worn out over its active years considering its current calculated isentropic efficiency of 30% and reported isentropic efficiencies of 71.2% and 71.5% in the literature [33,34]. In order to represent single flash GEPPs better and make the hybridization efforts meaningful, within the context of this article, the isentropic efficiency of the steam turbine is assumed to be 80%, which is in line with the typical isentropic efficiencies of geothermal steam turbines suggested by DiPippo [33].

KZD-1 is a typical single flash GEPP with multiple production wells whose schematic is supplied in Figure 1. Although a non-condensable gas (NCG) extraction system exists

 doi:10.20944/preprints202105.0542.v1

in reality, it is excluded within the context of this article to focus on thermodynamic modeling. After the two-phase geothermal brines are collected and flashed to 0.438 MPa and 146.9 °C, the geothermal brine and steam are separated through the high pressure (HP) separator. The geothermal brine is used for district heating before being directed to the neighboring Kızıldere-2 (KZD-2) GEPP's low pressure (LP) separator where it is ultimately re-injected. The geothermal steam after the HP separator at 146.91°C having flow rate of 19.45 kg s^{-1}, passes through the steam turbine, and exhaust steam is condensed through the direct contact (DC) steam condenser. The condensed steam is then pumped to the wet cooling tower (WCT) where it is used as cooling water and ultimately evaporates. The WCT uses no make-up water since the geothermal condensate is used as cooling water.

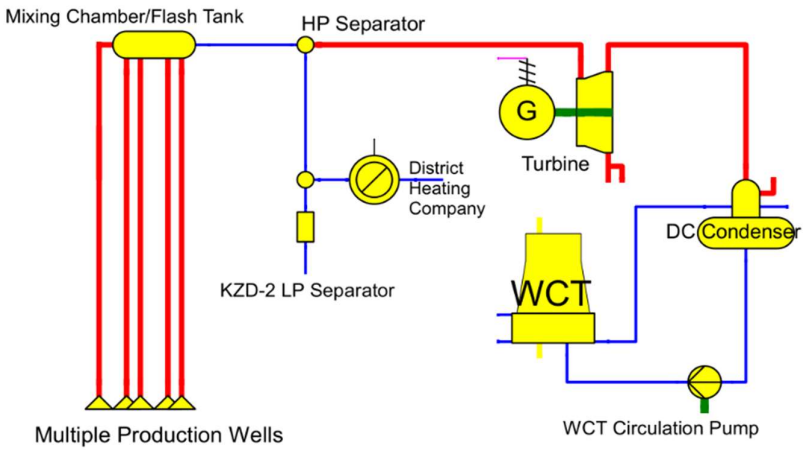

Figure 1. Existing schematic of KZD-1 GEPP as drawn in EBSILON®Professional.

2.1.2. Biomass Fuel Source

KZD-1 GEPP is located on the border of two western Anatolian cities of Turkey, Aydın and Denizli. In this region, the olive oil sector is well-developed [35]. Olive residue (OR) is a by-product of olive oil production and found abundantly in the region where it is mostly used for domestic heating [36]. To exploit the synergistic colocation of the two renewable energy resources, OR samples from an olive oil factory nearby KZD-1 GEPP were collected. The results of the conducted analyses of the OR are presented in Table 1.

Table 1. Analysis of the biomass fuel.

Parameter	
Proximate analysis (wt.%, dry basis)	
Volatile matter	83.9
Fixed Carbon [a]	14.2
Ash	1.9
Moisture content (wt.%, as received)	
Moisture	7.5
Ultimate analysis (wt.%, dry ash free)	
C	51.5
H	6.2
N	0.7
S	-
O [a]	41.6

 doi:10.20944/preprints202105.0542.v1

Table 1 (continued).

Calorific value	
Higher heating value (dry basis) [b] (MJ kg^{-1})	20.5
Lower heating value (wet basis) [c] (MJ kg^{-1})	17.5

[a] Calculated by difference
[b] Calculated by empirical correlation [37]
[c] Calculated by empirical correlation [32]

The higher heating value (HHV) of the biomass fuel is calculated based on its ultimate analysis following the procedure supplied by Sheng and Azevedo [37]. Lower heating value (LHV) is calculated from the HHV in parallel with the work of Manente and Lazzaretto [32]. As a cross check for HHV, Magãlhaes et al. [38] reported the HHV of their OR sample collected from Balıkesir region of Turkey as 20.11 MJ kg^{-1}, which is in a good agreement with the calculated HHV for the OR samples used in this article. Ultimate analysis and heating values of the biomass fuel are used as inputs to simulation software EBSILON®Professional where the hybrid power plant is modeled.

2.1.3. Model Development

A thermodynamic model is developed using EBSILON® Professional software for the application of the proposed novel hybridization scheme to KZD-1 GEPP. The thermodynamic concepts of the associated model are highlighted in Figure 2. The proposed hybrid scheme consists of following three cycles:

1. BTC: Biomass combustion driven sCO2 Topping Cycle;
2. BBC: Bottoming Biomass combustion and topping cycle waste heat driven steam Rankine Cycle;
3. EGC: Existing open-loop steam Rankine cycle driven by geothermal energy (EGC).

Here combination of BTC and BBC forms the new biomass combined cycle (BCC). Note that the conceptualization in Figure 2 is strictly for thermodynamic modeling and enables the thermal efficiencies for the BCC, BTC, and BBC to be calculated.

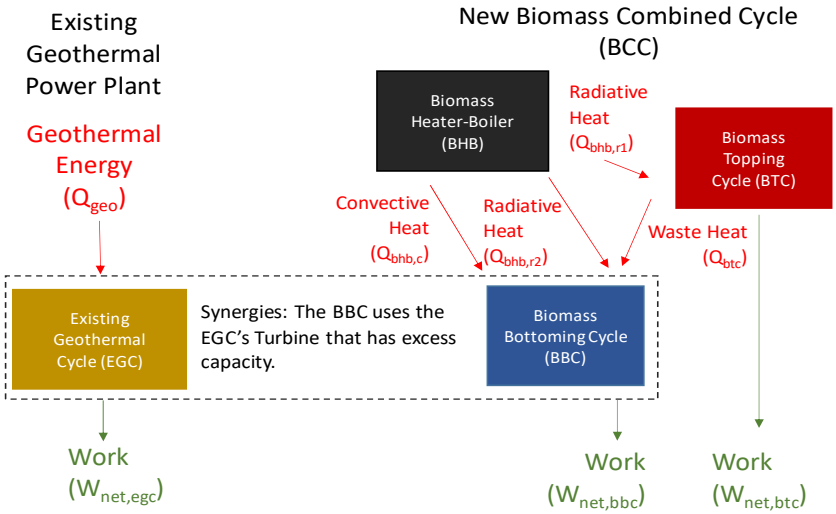

Figure 2. Thermodynamic conceptualization of proposed hybrid power plant.

In terms of thermodynamic modeling, the most prominent feature of the existing KZD-1 GEPP is that it utilizes an open-loop (not cyclic) steam Rankine cycle since the condensate outlet of the DC condenser is used as cooling water in WCT and eventually lost due to evaporation. The flow rate of this lost cooling water is equal to the original geothermal steam separated by the HP separator which then passes through the steam

 doi:10.20944/preprints202105.0542.v1

turbine of KZD-1 as shown in Figure 1. Due to this condition of the KZD-1 GEPP, sharing unused capacity of the existing cooling system is specifically avoided for the application of the proposed novel hybrid plant scheme to KZD-1. In other words, the existing cooling system of KZD-1 is not used to avoid losing biomass derived dry steam eventually through the WCT. For this purpose, a hypothetical steam Rankine bottoming cycle (BBC) is introduced to form a closed-loop biomass combined cycle (BCC) along with the biomass topping cycle (BTC). Although the hypothetical BBC and EGC are shown separately in Figure 2, they are not physically separate as both cycles share the existing steam turbine of KZD-1. Specifically, BBC is a theoretical construct to model a closed loop BCC. While BTC rejects its waste heat to BBC as shown in Figure 2, heat rejection from BBC is to the surroundings and achieved by means of a hypothetical dry cooling system shown in the overall hybrid power plant layout in Figure 3.

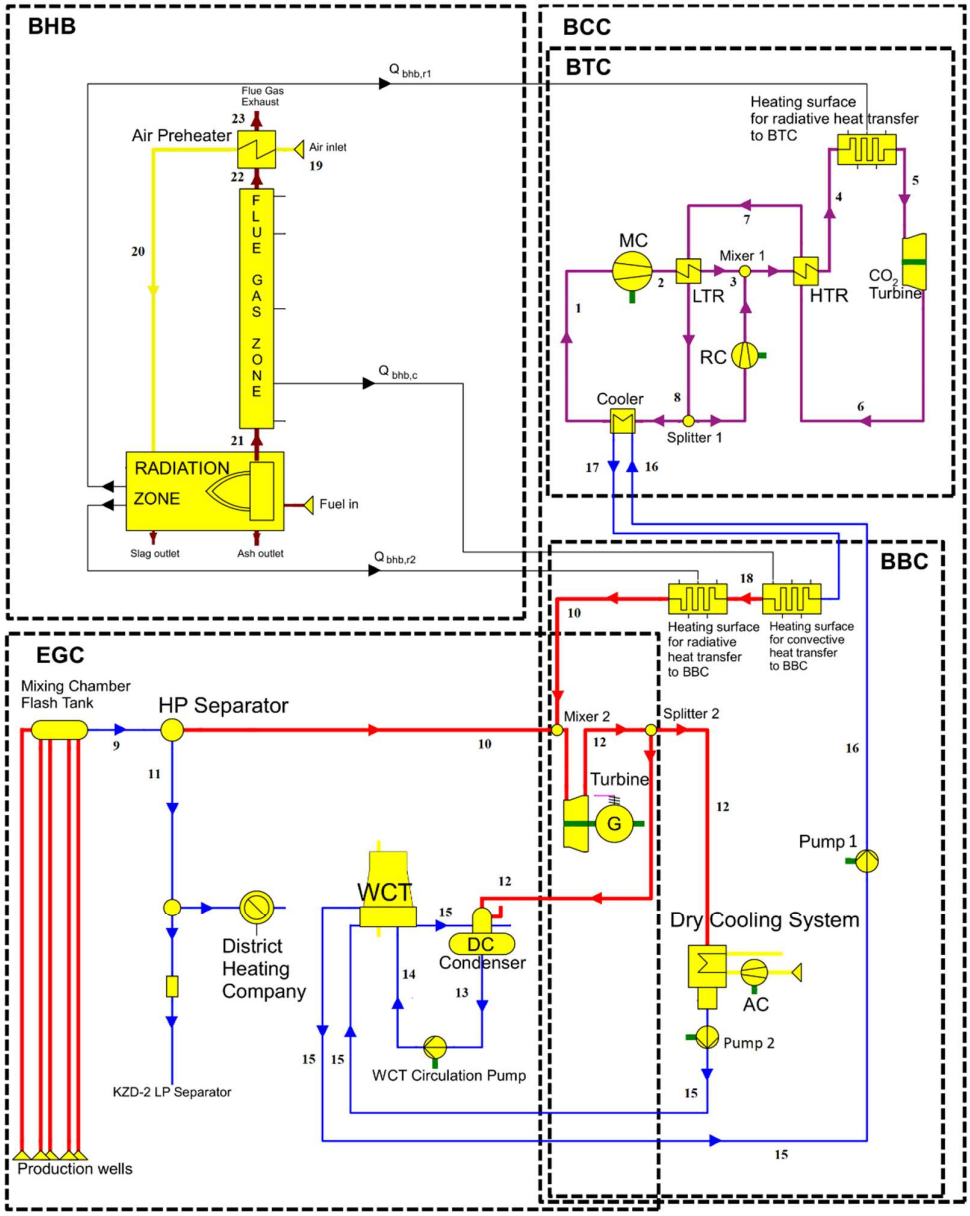

Figure 3. Schematic of the developed hybrid plant in EBSILON®Professional.

If EGC were to be a closed-loop cycle, there would be no need to construct the hypothetical BBC since EGC could be used as the bottoming cycle. Overall, application of the proposed novel hybridization scheme to KZD-1 GEPP resulted in two hypothetical cycles, i.e., BTC and BBC, whose combination constitutes fully biomass driven closed-loop combined cycle, BCC. The configuration of the hybrid plant is presented in Figure 3.

The topping part-flow sCO2 cycle used for hybridization (BTC) is adapted from the work of Utamura [21]. The characteristics of the optimized BTC are presented in Table 2. The turbine inlet condition is fixed at 550 °C and 20 MPa to be parallel with the part-flow sCO2 cycles designs in the literature [32,39–43]. The heat rejection from BTC is done to the BBC through the cooler. Heat input to BTC is achieved by means of radiative heat transfer from the biomass heater-boiler (BHB).

Since the existing steam Rankine cycle driven by geothermal energy (EGC) is open-loop and has the operating conditions mentioned in Section 2.1.1, a new closed loop hypothetical steam Rankine cycle (BBC) driven by biomass heat and waste heat from BTC is developed as follows. The working fluid, water at 0.1 MPa and 29 °C (State 15), is taken from the basin of the KZD-1 WCT and pumped to a pressure slightly higher than the steam turbine inlet pressure (State 16) to account for the subsequent pressure losses. Using the rejected heat from BTC via its cooler, water is sensibly preheated to a temperature of 127.7 °C (State 17) close to its saturation temperature of 146.9 °C. The preheated water at State 17 is heated with the radiation from the biomass combustion until it reaches 40% steam quality (State 18) and brought to dry steam phase (State 10) by the convective heat transfer from the flue gas. Then, it is mixed with the geothermal steam at Mixer 2 and is allowed to pass through the steam turbine. After passing through the turbine, the biomass sourced fraction of the exhaust steam is extracted through the Splitter 2 (State 12), condensed, and sensibly cooled via the hypothetical dry cooling system before it is pumped into the basin of the WCT at the same thermodynamic state it is originally taken from (State 15). The partial extraction of steam exhaust at Splitter 2 and its dry cooling are particularly done to avoid water consumption and create a closed-loop steam Rankine cycle, BBC. EGC and BBC are not physically separate as both cycles use the same steam turbine. The co-occurrence of these two cycles starts at the Mixer 2 and lasts until the biomass derived portion of the steam exhaust is extracted through Splitter 2 at State 12. BBC is used to provide additional dry steam to the steam turbine which before hybridization is operating under capacity. Since the heat supplied to BBC is purely derived from biomass, the additional power production of the steam turbine resulted due to the addition of dry steam and is attributed to the BBC.

The radiative-convective counter-current heater configuration from the work of Manente and Lazzaretto is modified and adapted to this article to drive both BTC and BBC [32]. Since the biomass combustion heat is used to add heat to the supercritical working fluid of BTC, and to create dry steam for BBC, this heating element is named as the Biomass Heater and Boiler (BHB). An alternative schematic of the BHB is shown in Figure 4 with state numbers compatible with the Figure 3. BHB can be considered as a discrete element from the cycles whose duty is to supply the heat required by BTC and BBC. The radiation from the biomass combustion is used to add heat to BTC inside the radiative section of BHB. As described above, the working fluid of BBC, water, which is previously preheated through the BTC cooler, is brought to 40% steam quality using the radiation from the combustion in the radiative section of BHB. The water-steam mixture at 40% steam quality is then brought to dry steam phase by means of convective heat transfer from the flue gas before being mixed with the geothermal steam in Mixer 2. The remaining low temperature useful heat in the flue gas is recovered using a counter-current air preheater. Finally, the flue gas is sent to the exhaust at 110°C, which is greater than the dew point to prevent condensation.

Preprints (www.preprints.org) | NOT PEER-REVIEWED | Posted: 24 May 2021 doi:10.20944/preprints202105.0542.v1

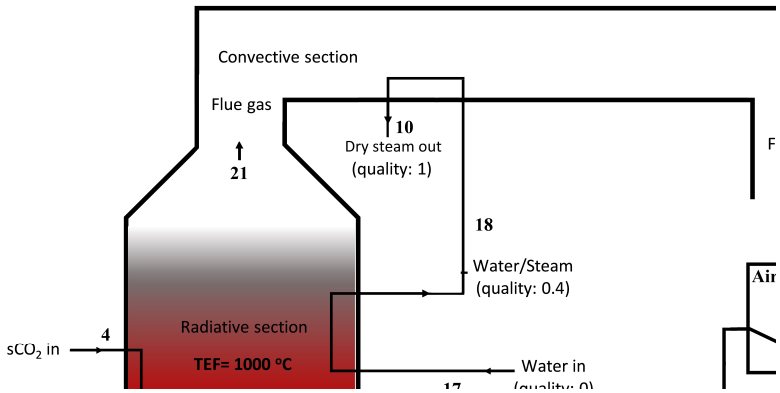

Figure 4. Radiative-convective counter-current heater-boiler (BHB) layout.

Table 2. Constants and inputs for the proposed hybrid plant.

Input	Value	Unit	Description	Source/Comment
BTC				
η_{comp}	90	%	Isentropic efficiency of the compressors	[21,32]
η_{turb}	93	%	Isentropic efficiency of the turbine	[21,31,44]
T_{turb}	550	°C	Turbine inlet temperature	[22,32,42,45]
P_{turb}	20	MPa	Turbine inlet pressure	[21]
φ	3	-	Expansion ratio of the CO_2 turbine, P_5/P_6	Optimized parameter [21].
ψ	0.75	-	Part-flow ratio, $\dot{m}_1/\dot{m}_8$	Optimized parameter [21].
ε_{recup}	96	%	Effectiveness of the recuperators	[21,39,46]
ε_{cooler}	80	%	Effectiveness of the cooler	[21,46]
$\Delta P_{hot,recup}$	0.03	MPa	Pressure drop at hot side of recuperators	[21,47]
$\Delta P_{cold,recup}$	0.22	MPa	Pressure drop at cold side of recuperators	[21,47]
$\Delta P_{hot,cooler}$	0.6	MPa	Pressure drop at hot side of cooler	[21,47]
$\Delta P_{cold,cooler}$	0.1	MPa	Pressure drop at cold side of cooler	[21,47]
$\Delta P_{bhb,co2}$	0.24	MPa	Pressure drop for CO_2 inside BHB	[21,47]
BBC				
$\eta_{turb,bot}$	80	%	Isentropic efficiency of the steam turbine	Assumption. See 2.1.1.
η_{pump}	80	%	Isentropic efficiency of the pumps	Generic value.
$\eta_{air\ comp}$	90	%	Isentropic efficiency of the air compressor	Generic value.
$T_{turb,bot}$	146.9	°C	Turbine inlet temperature	Operational KZD-1 data.
P_{turb}	0.438	MPa	Turbine inlet pressure	Operational KZD-1 data.
$\Delta P_{bhb,water}$	0.01	MPa	Pressure drop for water inside BHB	Generic value.
BHB				
λ	1.5	-	Excess air ratio	[32]
TEF	1000	°C	Effective temperature of radiation	[32]
Rad. loss	5	%	Heat loss in the radiative section of BHB	[32]
$\varepsilon_{air\ preheater}$	80	%	Effectiveness of the air preheater	[46]
$T_{air,in}$	20	°C	Air inlet temperature to air preheater	[32]

2.1.3. Energy Analysis

The thermodynamic modeling of the proposed hybrid configuration in Figure 3 is performed using EBSILON®Professional software and its EbsBoiler module. The design conditions and characteristics of the components are presented in Table 2. Due to the novelty of the proposed hybrid configuration, the well-known energetic performance parameters are slightly different than their standalone definitions and are defined as follows.

The heat inputs to cycles shown in Figure 2 are defined sequentially as:

 doi:10.20944/preprints202105.0542.v1

$$\dot{Q}_{bhb,r1} = \dot{m}_4 \, (h_5 - h_4) \quad (1)$$

$$\dot{Q}_{bhb,r2} = \dot{m}_{17} \, (h_{18} - h_1) \quad (2)$$

$$\dot{Q}_{bhb,c} = \dot{m}_{17} \, (h_{18} - h_{17}) \quad (3)$$

$$\dot{Q}_{btc} = \dot{m}_{17} \, (h_{17} - h_{16}) \quad (4)$$

where $\dot{Q}_{bhb,r1}$ and $\dot{Q}_{bhb,r2}$ are the radiative heat transfer from BHB to BTC and BBC, respectively. While $\dot{Q}_{bhb,c}$ represents the convective heat transfer from BHB to BBC, $\dot{Q}_{btc}$ represents the waste heat rejection from BTC cooler to BBC.

The net power outputs of the cycles are defined as:

$$\dot{W}_{net,btc} = \dot{W}_{turb,btc} - \dot{W}_{MC,btc} - \dot{W}_{RC,btc} \quad (5)$$

$$\dot{W}_{net,bbc} = \dot{W}_{turb,bbc} - \dot{W}_{dry\ cooling\ sys,bbc} \quad (6)$$

$$\dot{W}_{net,bcc} = \dot{W}_{net,bbc} + \dot{W}_{net,btc} \quad (7)$$

Consequently, the thermal efficiencies are calculated as:

$$\eta_{btc} = \frac{\dot{W}_{net,btc}}{\dot{Q}_{bhb,r1}} \quad (8)$$

$$\eta_{bbc} = \frac{\dot{W}_{net,bbc}}{\dot{Q}_{bhb,r2} + \dot{Q}_{bhb,c} + \dot{Q}_{btc}} \quad (9)$$

$$\eta_{bcc} = \frac{\dot{W}_{net,bcc}}{\dot{Q}_{bhb,r1} + \dot{Q}_{bhb,r2} + \dot{Q}_{bhb,c}} \quad (10)$$

Note that $\dot{Q}_{btc}$ is not present in the denominator of Eq. (10) due to representing an internal heat transfer within the combined cycle, BCC.

The biomass heater-boiler (BHB) efficiency representing the efficiency of the heat transfer from chemical biomass energy to BCC is defined in terms of a direct method as:

$$\eta_{bhb} = \frac{\dot{Q}_{bhb,r1} + \dot{Q}_{bhb,r2} + \dot{Q}_{bhb,c}}{\dot{m}_{fuel} \, LHV_{fuel}} \quad (11)$$

where $\dot{m}_{fuel}$ and LHV_{fuel} are the biomass fuel consumption and LHV of the biomass fuel, respectively.

Finally, the biomass to electricity conversion efficiency, η_{b2e}, can either be found with the multiplication of η_{bcc} and η_{bhb}, or explicitly from:

$$\eta_{b2e} = \frac{\dot{W}_{net,bcc}}{\dot{m}_{fuel} \, LHV_{fuel}} \quad (12)$$

2.1.4 Model Verification

Although it is not possible to verify the proposed hybrid power model due to its novelty, its constituting elements can be verified separately. The EGC model is verified using the actual operating power plant data supplied by Zorlu Energy. Two standalone part-flow sCO2 cycles are modeled in EBSILON®Professional using the design parameters supplied by Utamura [21] and Mecheri and Moullec [31]. T-s diagrams of the verification models are verified against the T-s diagrams supplied by Utamura [21] and Mecheri and Moullec [31] in Figure 5. Calculated first law efficiencies of 44.6% and 39% for the

Preprints (www.preprints.org) | NOT PEER-REVIEWED | Posted: 24 May 2021 doi:10.20944/preprints202105.0542.v1

verification models of these two respective studies are in line with their reported values of 45% and 39%.

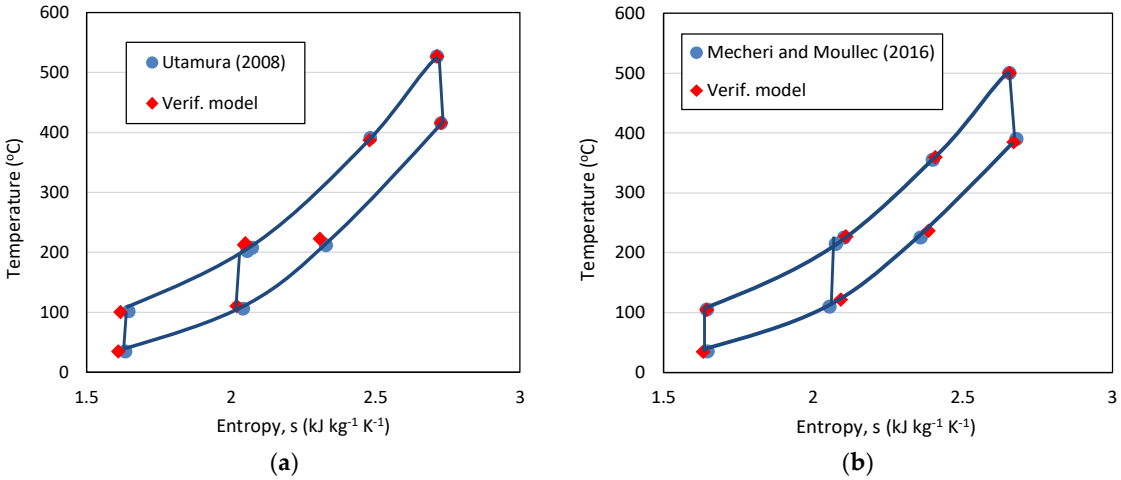

Figure 5. T-s diagrams of the standalone part-flow sCO2 cycle verification models against the models in the literature: (**a**) Verification against Utamura [21]; (**b**) Verification against Mecheri and Moullec [31].

The verification of the radiative-convective BHB model is done by creating a verification combustion model in EbsBoiler module of EBSILON® Professional for the different cases presented in the study of Manente and Lazzaretto [32]. The verification results are presented in Table 3 for 1 kg s^{-1} woody biomass fuel used in their work. Note that the effective temperature of radiation (TEF) and the heat loss in the radiative section is assumed as 1000 °C and 5% respectively, throughout this article to be consistent with Manente and Lazzaretto [32].

Considering the match in the T-s diagrams, consistency in thermal efficiencies, and the maximum absolute error of 2.3% in the BHB verification results, the proposed hybrid configuration in this article is assumed to be modeled accurately.

Table 3. BHB verification results based on the model of Manente and Lazzaretto [32].

	Inputs		Outputs					
	λ	T_{air} (°C)	$T_{flue\ gas}$ (°C)	$m_{flue\ gas}$ (kg s^{-1})	X_{CO2}	X_{H2O}	X_{N2}	X_{O2}
Manente and Lazzaretto [31]								
	1.5	20	1405	8.225	0.1826	0.0754	0.6738	0.0682
		100	1457					
	2.37	20	1000	12.41	0.1211	0.0499	0.7053	0.1237
	2.56	100	1000	13.33	0.1127	0.0465	0.7095	0.1313
Verification model								
	1.5	20	1407	8.273	0.1820	0.0749	0.6752	0.0679
		100	1458.6					
	2.37	20	999.9	12.49	0.1230	0.0496	0.7065	0.1209
	2.56	100	1000.7	13.41	0.1125	0.0462	0.7107	0.1306
Error:			0.1%	0.6%	-0.3%	-0.7%	0.2%	-0.4%
(Model-Ref.)/Ref.			0.1%					
			0.0%	0.6%	1.6%	-0.6%	0.2%	-2.3%
			0.1%	0.6%	-0.2%	-0.6%	0.2%	-0.5%

Preprints (www.preprints.org) | NOT PEER-REVIEWED | Posted: 24 May 2021 doi:10.20944/preprints202105.0542.v1

2.1.5 Optimization of input parameters

For their sCO2 cycle design for waste heat recovery systems, Manente and Fortuna [47] states that one of the main novelties in the recent literature on hybrid plant layouts is the sharing of some equipment to reduce the number of components. The efforts in this article aim to use the existing infrastructure of the KZD-1 GEPP to the fullest extent through the share of the existing steam turbine of KZD-1 with EGC and BBC. Concurrently, hybridization scenarios where the design operating conditions of the existing KZD-1 GEPP are changed by means of increased steam turbine inlet temperature or generation of superheat steam through biomass combustion are particularly avoided as power plant operators are generally not willing to make changes in their design conditions. In this sense, the hybridization exploits the excess steam turbine capacity resulting from the degradation in mass flow of the geothermal steam over the years by using the dry steam derived from biomass combustion in BBC to partially return the steam turbine to its design operating conditions. The mass flow rate of this additional biomass derived dry steam is equal to the mass flow rate of the BBC working fluid, water.

The first optimization is done on the flow rates of BBC and BTC by conducting a two-dimensional parametric analysis with three-dimensional output as presented in Figure 6. In this analysis, mass flow rate of the BTC is varied from 20 to 50 kg s^{-1} in equal 5 kg s^{-1} increments, while BBC mass flow rate is varied from 6 to 18 kg s^{-1} in even 2 kg s^{-1} increments. The reason BTC flow rate is included in this parametric analysis is that BTC is thermally coupled to the BBC. The input parameters of these two cycles are held constant and equal to the values in Table 2, except for part-flow ratio, ψ, and turbine expansion ratio, φ, of BTC. The base inputs for ψ and φ are taken as 2.51 and 0.68, respectively, as suggested by Utamura [21], and are optimized after the mass flow rates are determined.

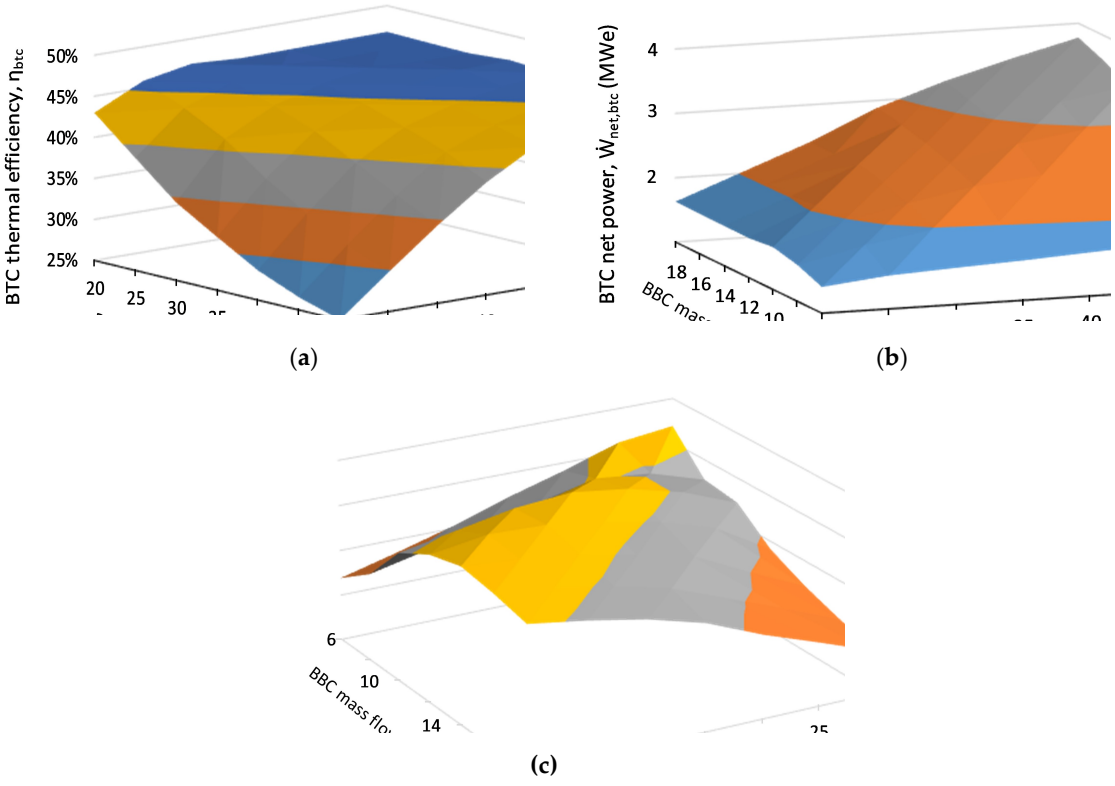

Figure 6. Results of parametric analysis conducted on the flow rates of BTC and BBC. (**a**) BTC thermal efficiency, η_{btc} ; (**b**) BTC net power output, $\dot{W}_{net,btc}$; (**c**) BCC thermal efficiency, η_{bcc}.

There are two main outcomes of the conducted analysis in Figure 6. First, the thermal efficiency of BCC in Figure 5 (c) shows a minima for the maximum flow rate of BTC at 50

 doi:10.20944/preprints202105.0542.v1

kg s^{-1} and minimum flow rate of BBC at 6 kg s^{-1}. The underlying reason leading to this result is the increase of the main compressor (MC) inlet temperature (State 1) of BTC. The increase in MC inlet temperature is directly proportional to BTC flow rate while being inversely proportional to BBC flow rate for a fixed effectiveness value of the BTC cooler since the working fluid of BBC acts as a heat rejection medium for BTC. Note that the reason of utilizing CO_2 as a working fluid in a closed-loop power cycle is to exploit the thermophysical properties of CO_2 requiring minimum compression work in the vicinity of its critical temperature of 31.1 °C [48]. Therefore, the efficiency drops as the MC inlet temperature increases. This behavior is also prominent in Figure 6 (a) where topping cycle efficiency severely drops to 25%. Second, the BCC thermal efficiency exhibits another minima for the minimum flow rate of BTC at 20 kg s^{-1} and maximum flow rate of BBC at 18 kg s^{-1}. Note that the BTC thermal efficiency is maximum for this flow rate pair in Figure 6 (a), whereas BBC thermal efficiency is independent of the flow rates owing to its fixed intensive thermodynamic properties defined by the KZD-1 steam turbine inlet temperature and constant ambient temperature. The underlying theory leading to this minima in BCC for this flow rate pair is the increase in the power generation share of BBC which has a lower thermal efficiency compared to BTC.

The motivation for the flow rate selection procedure is to maximize BCC thermal efficiency while keeping the scale of BTC as small as possible to minimize the additional equipment cost. Therefore, the flow rate pair of 45 kg s^{-1} and 12 kg s^{-1}, is selected for BTC and BBC, respectively. The mass flow rate of the total steam feeding the KZD-1 steam turbine increases from 19.45 kg s^{-1} to 31.45 kg s^{-1} with the addition of the biomass derived dry steam and brings KZD-1 turbine close to its operation conditions in 2004 [34].

The two-characteristic parameters of BTC, namely part-flow ratio, ψ, and turbine expansion ratio, φ, are optimized upon the decision of the flow rates. The part-flow ratio represents the ratio of the flow entering main compressor to the total flow; therefore, its unit value represents a simple-recuperated cycle. On the other hand, turbine expansion ratio, φ, is the ratio of the turbine inlet pressure to turbine outlet pressure. These ratios do not only affect the cycle level performance parameters such as the thermal efficiency but also dictate the component level indicators such as the heat duty and pinch point of the recuperators under the condition of having constant effectiveness. Optimizations on these ratios are conducted and results are presented in Figures 7 and 8. First, the part-flow ratio is varied from 0.6 to 1 in equal 0.05 increments while all other inputs are kept constant and equal to the values in Table 2, except for the turbine expansion ratio which is taken at its base value of 2.51 [21]. The part-flow ratio is selected as 0.75 to have the maximum BCC efficiency and minimum cumulative heat duty for the recuperators while at least 5°C pinch point is ensured. Upon determination and fixing of ψ as 0.75, the turbine expansion ratio, φ, is varied from 2 to 4 in even 0.2 increments while keeping all other inputs equal to their values in Table 2. Similarly, the optimum φ as chosen and finalized as 3 to have the maximum possible BCC thermal efficiency and minimum cumulative recuperator heat duty where at least 5°C pinch point is ensured for each recuperator.

The last optimization is done on the intermediate steam quality of the BBC (State 18). Since BHB design is discrete from the cycles as discussed in Section 2.1.3., the intermediate steam quality does not affect the cycle parameters but used as a boundary condition to determine the size of radiative and convective sections of the BHB. The preheated water at State 17 is heated by means of radiative combustion heat up to this intermediate steam quality in the radiative section of BHB. In addition to determining the size of the radiative and convective sections of BHB, this intermediate quality controls the temperature of the flue gas utilized in the convective section of the BHB. The results of the parametric study conducted on this intermediate steam quality implies in Figure 9 that as more radiative heat is used to increase the intermediate steam quality, the temperature of the flue gas decreases. In order to keep the flue gas temperature below 1000 °C as suggested by Strzalka et al. [49] and have a typical heat distribution in the range of radiation chamber (45%-55%; convective section 45%-25%; stack and other heat losses: l0%-20% as suggested

Preprints (www.preprints.org) | NOT PEER-REVIEWED | Posted: 24 May 2021 doi:10.20944/preprints202105.0542.v1

by Stehlík et al. [50]), the intermediate steam quality is chosen as 0.4. Note that the limitation of the flue gas temperature below 1000 °C is achieved either by increasing the excess air ratio [32], or recirculating the flue gas inside the furnace [49] in the literature. In this article, the temperature control of the flue gas is controlled through the intermediate steam quality at State 18. However, a novel biomass heater-boiler design to supply heat to two power cycles having different working fluids is beyond the scope of this article and may require further investigation.

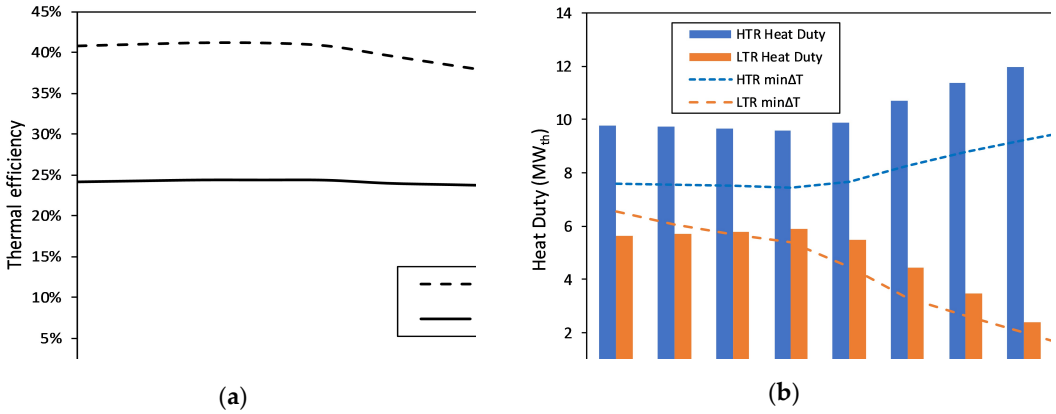

Figure 7. Optimization of part-flow ratio: **(a)** Variations in BTC and BCC thermal efficiencies with changing part-flow ratio; **(b)** Variations in the heat duties and pinch point of the recuperators with changing part-flow ratio.

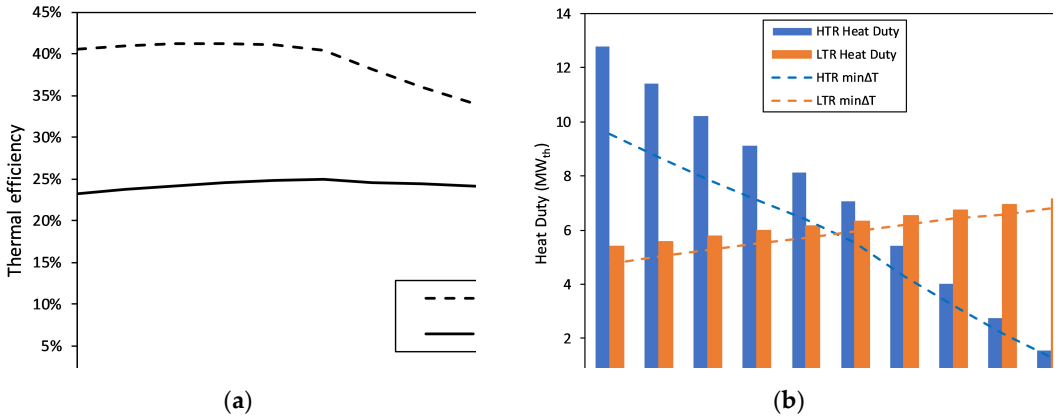

Figure 8. Optimization of turbine expansion ratio: **(a)** Variations in thermal efficiencies of BCC and BTC with changing turbine expansion ratio**; (b)** Variations in the heat duties and pinch point of the recuperators with changing turbine expansion ratio.

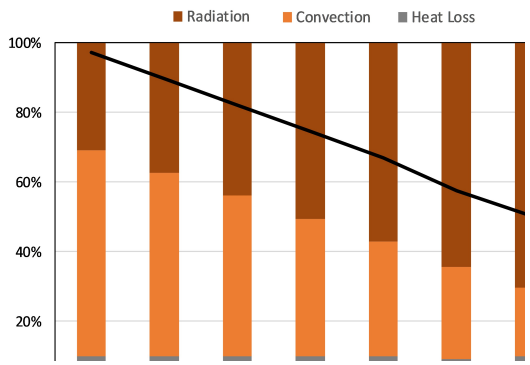

Figure 9. Heat transfer distribution and the flue gas temperature leaving the radiative section of the BHB (State 21) with varying intermediate steam quality.

 doi:10.20944/preprints202105.0542.v1

3. Results and Discussion

The energetic results of the cycles used in the hypothetical hybridization scenario of KZD-1 GEPP are presented in Table 4. The design parameters are provided in Table 2 for reproducibility of the results. T-s diagrams of BTC and BBC are shown in Figure 10.

Table 4. Energetic results of the cycles used in hybridization of KZD-1 GEPP.

Cycle	$\dot{m}$ *kg s^{-1}*	η_{th} %	$\dot{W}_{net}$ *MWe*
Topping part-flow sCO2 (BTC)	45	40.1	3.4
Bottoming steam Rankine (BBC)	12	16.9	5.3
Combined (BCC)	-	24.9	8.7

The thermal efficiency of the standalone part-flow sCO2 cycle having the same turbine inlet temperature (TIT) of 550°C as in this article are reported around 46.5% in the literature [22]. In this work it is expected that the efficiency of the topping sCO2 cycles to be penalized slightly to maximize the performance of the combined cycle. However, the efficiency penalty of more than 5% exceeds this expectation. For example, the part-flow sCO2 topping cycle in the study of Manente and Lazzaretto [32] has 44.2% thermal efficiency for the same maximum turbine inlet conditions as in this article. The underlying theory leading to an overly penalized BTC efficiency in this article is the deviation from optimum compressor inlet conditions at State 1. The sCO2 cycles takes advantage of the minimal compression work of the working fluid CO_2 at the vicinity of its critical temperature of 31.8°C. Note that the temperature of State 1 in this paper is 42.9°C which causes the T-s diagram of the topping cycle to shift slightly right of the saturation curve of CO_2 and ultimately decreases the cycle efficiency about 5% compared to results in the literature. The reason for the deviation from the optimum CO_2 compression inlet temperature is that the rejected heat of BTC is recovered in BCC using the coupling heat exchanger, cooler. As the flowrate of the BBC increases, the temperature of the CO_2 at the hot side outlet of cooler (State 1) increases under a fixed effectiveness value of the cooler. Although this process penalizes the efficiency of BTC around 5%, it allows utilization of 5 MW thermal heat in the bottoming cycle. In fact, the scale of the topping cycle is desired to be kept as small as possible to use the existing steam turbine of KZD-1 to the fullest extent by BBC. Therefore, the efficiency drop of BTC is diluted in the combined cycle due to utilization of significant portion of the biomass derived heat in BCC as shown in Figure 11. As a comparison, the net power distribution in the work of Manente and Lazzaretto [32] favors topping cycle by 90% (topping) to 10% (bottoming), while bottoming cycle is favored in this article by 61% (bottoming) to 39% (topping).

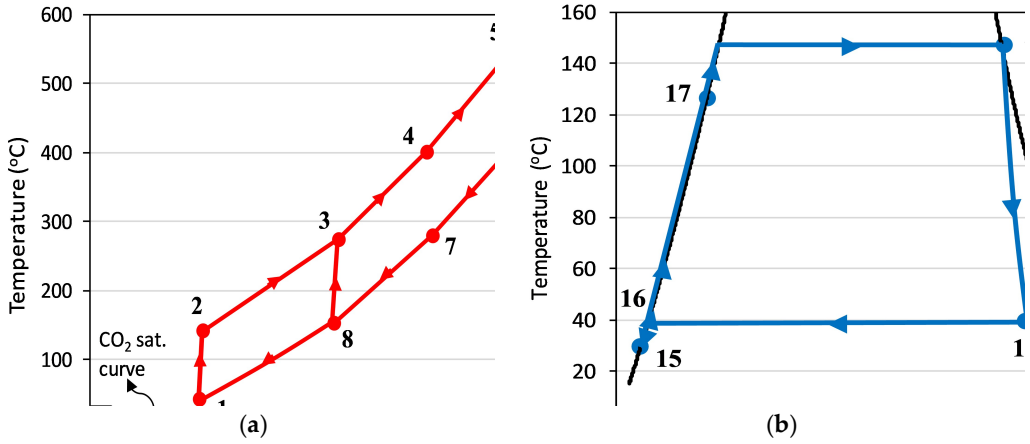

Figure 10. T-s diagrams of the thermodynamic cycles used in hybridization of KZD-1 GEPP: (**a**) BTC; (**b**) BBC.

 doi:10.20944/preprints202105.0542.v1

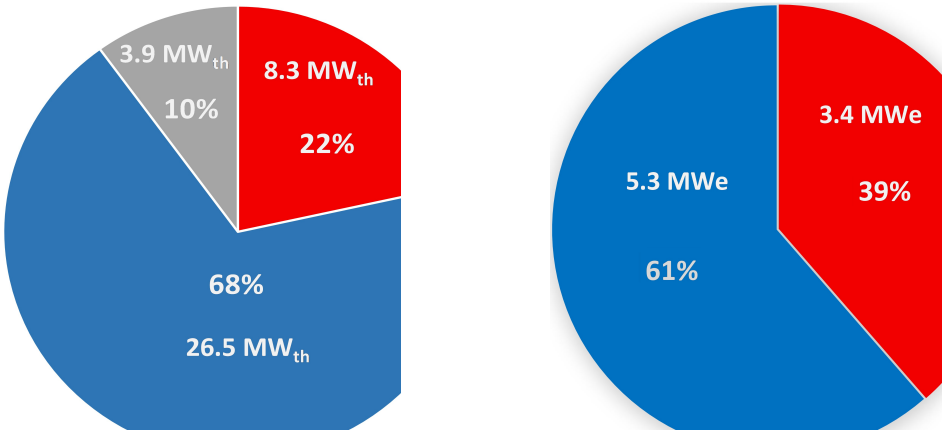

(**a**) (**b**)

Figure 11. Heat and power distribution between the cycles: (**a**) Allocation of biomass energy; (**b**) Net power distribution.

The thermal efficiency of the single flash GEPPs having TIT of 150°C lies in the range of 15-18% in the literature [51]. Although the 16.9% thermal efficiency of BBC falls in this range, 24.9% thermal efficiency of BCC can be considered to be penalized in itself due to favoring BBC in biomass energy utilization as seen in Figure 11 (a). There is no similar combined cycle configuration in the literature where sCO2 and steam Rankine cycles are utilized in cascaded manner as in this article to allow comparison for BCC thermal efficiency. However, Jiang et al. reported their hybrid solar thermal–EGS power plant using CO_2 as working fluid as 21.93% and 22.44%, respectively for TITs of 500 °C and 600 °C, which is in relatively good agreement with the found BCC efficiency [15]. On the other hand, Manente and Lazzaretto reports their biomass to electricity conversion efficiency as 34.3% for their combined cycle [32]. Despite their topping cycle being a part-flow sCO2 cycle with the same turbine inlet conditions as in this article, it should be noted that their bottoming cycle is a simple recuperated sCO2 cycle having a TIT of 313.9 °C while the TIT of the bottoming steam Rankine cycle in this article is restricted by the operational TIT of KZD-1 GEPP at 146.9 °C. Therefore, lower biomass to electricity conversion efficiency in this article is expected compared to their 34.3% conversion efficiency.

Within the scope of this article, the mass flow rate of the biomass fuel in BHB is adjusted such that the temperature of the exhaust flue gas at air preheater outlet (State 23) is limited at the minimum allowable temperature of 110 °C to prevent dew point condensation after the demanded heat is supplied to the combined cycle [31]. Results of the BHB parameters including flue gas mass flow rate, flue gas temperature leaving the radiative section of BHB at State 21, flue gas composition, calculated adiabatic flame temperature, and the BHB efficiency are presented in Table 5. Based on the mass flow rate of the biomass fuel, the biomass to electricity conversion efficiency is calculated as 22.4% using Eq. (12).

Table 5. Radiative-convective counter-current heater-boiler (BHB) results.

η_{bhb}	$\dot{m}_{fuel}$ (kg s^{-1})	$\dot{m}_{flue\ gas}$ (kg s^{-1})	TAF (°C)	T_{21} (°C)	X_{CO2}	X_{H2O}	X_{N2}	X_{O2}
0.90	2.2	21.5	1623	890.6	0.1775	0.0623	0.6909	0.0693

Even though this paper lacks economic and exergy analysis, preliminary remarks can be made on the Q-T diagrams of the heat exchangers presented in Figure 12. For the recuperators, it is assured that no pinch problem exists, and the minimum temperature difference between two streams is kept larger than 5 °C with effectiveness of 96%. Although it is expected for the recuperators to have a good temperature match between the cold and hot flows due to having the same working fluid on both sides, the good temperature

 doi:10.20944/preprints202105.0542.v1

match for the cooler is promising in terms of low potential of exergy destruction and stems from the fact that water is sensibly heated through the cooler. Since the cooler acts as a thermal coupling mechanism between BTC and BBC, it can be suggested that a good synergy between two intrinsically different cycles is achievable.

The heat addition to BTC in this article is only possible between state points 4 and 5 in Figure 11 (a) owing to the highly recuperative characteristics of the sCO2 cycles. Thus, the heat below a certain temperature, i.e., 400°C in this article, cannot be utilized in the topping sCO2 cycle without changing its layout or adding additional heat exchangers. In order to overcome this problem, sCO2 cycles are generally utilized in the literature in cascaded manner as mentioned in Section 1 and 2. Since the heat of the flue gas below 400°C is utilized in BBC through the convective section of BHB, the problem of having complex sCO2 cycle layout or adding another sCO2 cycle as a bottoming cycle is resolved. Finally, UA values (commonly known as conductance and expressed in units of kW K^{-1}) for each heat exchanger are supplied as a preliminary economic indicator. Assumed that equipment cost scale with the UA value, recuperators appear to be the heat exchanger units requiring most of the investment costs [44,47].

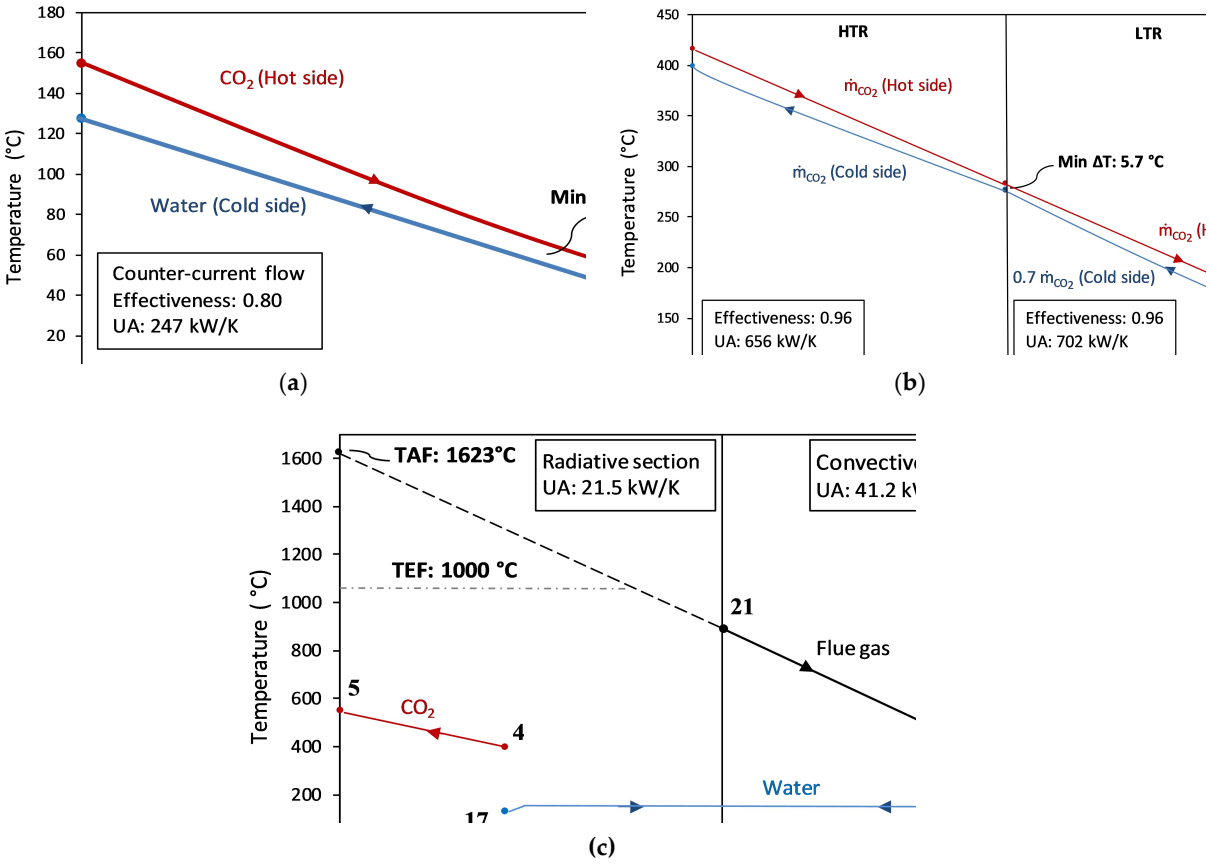

Figure 12. Q-T diagram of the heat exchangers. (**a**) Cooler; (**b**) Recuperators; (**c**) Radiative-convective counter-current heater-boiler (BHB) with assumed TEF=1000°.

4. Conclusions

In this article the underperforming KZD-1 GEPP is theoretically hybridized using a biomass driven sCO2 topping and steam Rankine bottoming cycles where locally sourced olive residue is used as a biomass fuel source. While a topping sCO2 cycle is specifically chosen for its potential for flexible electricity generation, as a first step to develop this novel hybridization scheme, only the steady-state design conditions of hybridization are

 doi:10.20944/preprints202105.0542.v1

modeled in this work. Transient scenarios for hourly fluctuations or seasonal variations can be investigated as a future work. The hybridization increases the nominal flow rate of the steam feeding the KZD-1 turbine from 19.45 s^{-1} to 31.45 s^{-1} and brings the steam turbine closer to its operating conditions reported in 2004 [34]. 3.4 MWe and 5.3 MWe additional net powers are generated through the topping and bottoming cycles having 40.1% and 16.9% thermal efficiencies, respectively. The combined cycle composed of the combination of topping and bottoming cycle has a thermal efficiency of 24.9% and net power generation of 8.7 MWe. Biomass to electricity conversion efficiency is calculated as 22.4% for a fuel consumption rate of 2.2 kg s^{-1}. Despite the penalties in topping cycle thermal efficiency and biomass to electricity conversion efficiency compared to literature, the motivation in hybridization scenario in this article is using the existing infrastructure of KZD-1 GEPP to the fullest extent by keeping the topping cycle and additional investments costs as small as possible while retaining the maximum possible efficiency. In this context, the goal of sharing existing components in hybrid power plant layouts is arguably achieved [47]. Moreover, the high temperature heat addition problem of sCO2 cycles is resolved by utilizing the heat of the flue gas under 400 °C in the bottoming cycle. Consequently, the need of adding a bottoming sCO2 cycle or having a complex sCO2 cycle layout is avoided.

Although this paper considers hybridization scenario of KZD-1 GEPP as a case study, the results can be adapted to different locations, e.g., to a single flash GEPP in Philippines using a rice husk as the fuel source. In fact, there would be no need to create a hypothetical bottoming steam Rankine cycle as in this article if such a single flash GEPP works in cyclic mode contrary to the open-cycle case of KZD-1 GEPP. In that case, the existing closed-loop steam Rankine cycle can be used as the bottoming cycle and offer even better thermal and cost efficiency since existing unused cooling system can be utilized and the need of an additional dry cooling system is eliminated.

Abbreviations/Nomenclature

b2e	biomass to electricity
BBC	biomass bottoming cycle
BCC	biomass combined cycle
BHB	biomass heater boiler
BTC	biomass topping cycle
CSP	concentrated solar power
DC	direct contact
DSG	direct steam generation
EGS	enhanced geothermal system
GEPP	geothermal electric power plant
HHV	higher heating value
HP	lower heating value
HTR	high temperature recuperator
KZD-1	Kızıldere-1
KZD-2	Kızıldere-2
LCOE	levelized cost of electricity
LHV	lower heating value
LP	low pressure
LTR	low temperature recuperator
MC	main compressor
NGC	non-condensable gas
OR	olive residue
ORC	organic Rankine cycle
PTC	parabolic trough collector
PV	photovoltaic
RC	recompressor

sCO2	supercritical CO_2
TAF	adiabatic flame temperature
tCO2	transcritical CO_2
TEF	effective temperature of radiation
TIT	turbine inlet temperature
WCT	wet cooling tower
WHR	waste heat recovery
λ	excess air ratio

Author Contributions: Conceptualization, B.M.; methodology, B.M.; software, B.M.; validation, B.M.; formal analysis, D.B.; investigation, D.B and F. K.; data curation, B.M.; writing—original draft preparation, B.M.; writing—review and editing, B.M., D.B. and F.K.; visualization, B.M. and D.B.; supervision, D.B. and F.K.; project administration, D.B.; funding acquisition, D.B. All authors have read and agreed to the published version of the manuscript.

Funding: This research is funded by EU H2020 Project GeoSmart: Technologies for geothermal to enhance competitiveness in smart and flexible operation under Grant Agreement number 818576.

Data Availability Statement: The data presented in this study are available on request from the corresponding author.

Acknowledgments: Authors would like to thank Zorlu Energy for their help on sharing operational data of their power plant.

Conflicts of Interest: The authors declare no conflict of interest.

References

1. Wendt, D.S.; Mines, G.L. Use of a geothermal-solar retrofit hybrid power plant to mitigate declines in geothermal resource productivity. *Trans. - Geotherm. Resour. Counc.* **2014**, *38*, 825–832.
2. Michaelides, E.E.; Michaelides, D.N. The effect of ambient temperature fluctuation on the performance of geothermal power plants. *Int. J. Exergy* **2011**, *8*, 86–98, doi:10.1504/IJEX.2011.037216.
3. Pasqualetti, M.J. The site specific nature of geothermal energy: the primary role of land use planning in nonelectric development. *Nat. Resour. J.* **1983**, *23*, 795–814.
4. Borsukiewicz-Gozdur, A. Dual-fluid-hybrid power plant co-powered by low-temperature geothermal water. *Geothermics* **2010**, *39*, 170–176, doi:10.1016/j.geothermics.2009.10.004.
5. Briola, S.; Gabbrielli, R.; Bischi, A. Off-design performance analysis of a novel hybrid binary geothermal-biomass power plant in extreme environmental conditions. *Energy Convers. Manag.* **2019**, *195*, 210–225, doi:10.1016/j.enconman.2019.05.008.
6. Rostamzadeh, H.; Gargari, S.G.; Namin, A.S.; Ghaebi, H. A novel multigeneration system driven by a hybrid biogas-geothermal heat source, Part II: Multi-criteria optimization. *Energy Convers. Manag.* **2019**, doi:10.1016/j.enconman.2018.11.035.
7. DiPippo, R. *Geothermal Power Generation: Developments and Innovation*; 2016; ISBN 9780081003442.
8. Li, K.; Liu, C.; Jiang, S.; Chen, Y. Review on hybrid geothermal and solar power systems. *J. Clean. Prod.* **2020**, *250*, 119481, doi:10.1016/j.jclepro.2019.119481.
9. Lentz, Á.; Almanza, R. Solar-geothermal hybrid system. *Appl. Therm. Eng.* **2006**, *26*, 1537–1544, doi:10.1016/j.applthermaleng.2005.12.008.
10. Lentz, Á.; Almanza, R. Parabolic troughs to increase the geothermal wells flow enthalpy. *Sol. Energy* **2006**, *80*, 1290–1295, doi:10.1016/j.solener.2006.04.010.
11. Mir, I.; Escobar, R.; Vergara, J.; Bertrand, J. Performance Analysis of a Hybrid Solar-Geothermal Power Plant in Northern Chile. *Proc. World Renew. Energy Congr. – Sweden, 8–13 May, 2011, Linköping, Sweden* **2011**, *57*, 1281–1288, doi:10.3384/ecp110571281.
12. Cardemil, J.M.; Cortés, F.; Díaz, A.; Escobar, R. Thermodynamic evaluation of solar-geothermal hybrid power plants in

northern Chile. *Energy Convers. Manag.* **2016**, *123*, 348–361, doi:10.1016/j.enconman.2016.06.032.

13. McTigue, J.D.; Castro, J.; Mungas, G.; Kramer, N.; King, J.; Turchi, C.; Zhu, G. Hybridizing a geothermal power plant with concentrating solar power and thermal storage to increase power generation and dispatchability. *Appl. Energy* **2018**, doi:10.1016/j.apenergy.2018.07.064.
14. Bonyadi, N.; Johnson, E.; Baker, D. Technoeconomic and exergy analysis of a solar geothermal hybrid electric power plant using a novel combined cycle. *Energy Convers. Manag.* **2018**, *156*, 542–554, doi:10.1016/j.enconman.2017.11.052.
15. Jiang, P.X.; Zhang, F.Z.; Xu, R.N. Thermodynamic analysis of a solar–enhanced geothermal hybrid power plant using CO2 as working fluid. *Appl. Therm. Eng.* **2017**, *116*, doi:10.1016/j.applthermaleng.2016.12.086.
16. Conboy, T.; Wright, S.; Pasch, J.; Fleming, D.; Rochau, G.; Fuller, R. Performance characteristics of an operating supercritical CO 2 brayton cycle. *J. Eng. Gas Turbines Power* **2012**, *134*, 1–12, doi:10.1115/1.4007199.
17. Conboy, T.; Pasch, J.; Fleming, D. Control of a supercritical CO2 recompression brayton cycle demonstration loop. *J. Eng. Gas Turbines Power* **2013**, *135*, 1–12, doi:10.1115/1.4025127.
18. Angelino, G. Carbon dioxide condensation cycles for power production. *J. Eng. Gas Turbines Power* **1968**, *90*, 287–295, doi:10.1115/1.3609190.
19. Utamura, M.; Hasuike, H.; Ogawa, K.; Yamamoto, T.; Fukushima, T.; Watanabe, T.; Himeno, T. Demonstration of Supercritical CO2 Closed Regenerative Brayton Cycle in a Bench Scale Experiment. In Proceedings of the Proceedings of ASME Turbo Expo; Copenhagen, Denmark GT2012-68697, 2012; pp. 1–10.
20. Turchi, C.S.; Ma, Z.; Dyreby, J. Supercritical carbon dioxide power cycle configurations for use in concentrating solar power systems. *Proc. ASME Turbo Expo* **2012**, *5*, 967–973, doi:10.1115/GT2012-68932.
21. Utamura, M. Thermodynamic analysis of part- flow cycle supercritical CO2 gas turbines. *Proc. ASME Turbo Expo* **2008**, *2*, 423–430, doi:10.1115/GT2008-50151.
22. Crespi, F.; Gavagnin, G.; Sánchez, D.; Martínez, G.S. Supercritical carbon dioxide cycles for power generation: A review. *Appl. Energy* 2017.
23. Wang, X.; Wu, Y.; Wang, J.; Dai, Y. Thermo-economic Analysis of a Recompression sCO2 Cycle Combined with a tCO2 Cycle. In Proceedings of the Proceedings of ASME Turbo Expo 2015: Turbine Technical Conference and Exposition GT2015; Montréal, Canada, 2015; pp. 1–11.
24. Wang, X.; Wang, J.; Zhao, P.; Dai, Y. Thermodynamic Comparison and Optimization of Supercritical CO2 Brayton Cycles with a Bottoming Transcritical CO2 Cycle. *J. Energy Eng.* **2016**, *142*, doi:10.1061/(ASCE)EY.1943-7897.0000292.
25. Wu, C.; Yan, X.J.; Wang, S. Sen; Bai, K.L.; Di, J.; Cheng, S.F.; Li, J. System optimisation and performance analysis of CO2 transcritical power cycle for waste heat recovery. *Energy* **2016**, doi:10.1016/j.energy.2015.12.001.
26. Besarati, S.M.; Yogi Goswami, D. Analysis of Advanced Supercritical Carbon Dioxide Power Cycles With a Bottoming Cycle for Concentrating Solar Power Applications. *J. Sol. Energy Eng.* **2014**, *136*, 1–7, doi:10.1115/1.4025700.
27. Zhang, H.; Shao, S.; Zhao, H.; Feng, Z. Gt2014-26500 Thermodynamic Analysis of a Sco 2 Part-Flow Cycle Combined With. **2014**, 1–8.
28. Wang, X.; Dai, Y. Exergoeconomic analysis of utilizing the transcritical CO2 cycle and the ORC for a recompression supercritical CO2 cycle waste heat recovery: A comparative study. *Appl. Energy* **2016**, *170*, 193–207, doi:10.1016/j.apenergy.2016.02.112.
29. Akbari, A.D.; Mahmoudi, S.M.S. Thermoeconomic analysis & optimization of the combined supercritical CO2 (carbon dioxide) recompression Brayton/organic Rankine cycle. *Energy* **2014**, *78*, 501–512, doi:10.1016/j.energy.2014.10.037.
30. Le Moullec, Y. Conceptual study of a high efficiency coal-fired power plant with CO2 capture using a supercritical CO2 Brayton cycle. *Energy* **2013**, *49*, 32–46, doi:10.1016/j.energy.2012.10.022.
31. Mecheri, M.; Le Moullec, Y. Supercritical CO2 Brayton cycles for coal-fired power plants. *Energy* **2016**,

doi:10.1016/j.energy.2016.02.111.

32. Manente, G.; Lazzaretto, A. Innovative biomass to power conversion systems based on cascaded supercritical CO2 Brayton cycles. *Biomass and Bioenergy* **2014**, doi:10.1016/j.biombioe.2014.07.016.
33. DiPippo, R. *Geothermal power plants*; 2012; Vol. 7; ISBN 9780080878737.
34. Gokcen, G.; Ozturk, H.K.; Hepbasli, A. Overview of Kizildere Geothermal Power Plant in Turkey. *Energy Convers. Manag.* **2004**, *45*, 83–98, doi:10.1016/S0196-8904(03)00129-8.
35. The Turkish Olive Oil Sector, Available Online. URL:https://www.olioofficina.it/en/knowledge/economy/the-turkish-olive-oil-sector.htm (accessed on 15 April 2021). URL: https://webdosya.csb.gov.tr/db/destek/icerikler/zeyt-n_sektoru_at-klar-n-n_yonet-m-_projes--20191127122437.pdf
36. Hocaoğlu, S.M.; Haksevenler, H.G.; Baştürk, İ.; Aydöner, C. *Zeytin Sektörü Atıklarının Yönetimi Projesi Nihai Rapor*; 2015; URL: https://webdosya.csb.gov.tr/db/destek/icerikler/zeyt-n_sektoru_at-klar-n-n_yonet-m-_projes--20191127122437.pdf
37. Sheng, C.; Azevedo, J.L.T. Estimating the higher heating value of biomass fuels from basic analysis data. *Biomass and Bioenergy* **2005**, *28*, 499–507, doi:10.1016/j.biombioe.2004.11.008.
38. Magalhães, D.; Kazanç, F.; Riaza, J.; Erensoy, S.; Kabaklı, Ö.; Chalmers, H. Combustion of Turkish lignites and olive residue: Experiments and kinetic modelling. *Fuel* **2017**, *203*, 868–876, doi:10.1016/j.fuel.2017.05.050.
39. Dostal, V.; Hajek, P. Proceedings of the 2014 22nd International Conference on Nuclear Engineering.; Prague, Czech Republic, 2014; pp. 1–7.
40. Wang, X.; Liu, Q.; Bai, Z.; Lei, J.; Jin, H. Thermodynamic Analysis of the Cascaded Supercritical CO2 Cycle Integrated with Solar and Biomass Energy. *Energy Procedia* **2017**, *105*, 445–452, doi:10.1016/j.egypro.2017.03.339.
41. Sun, E.; Xu, J.; Li, M.; Li, H.; Liu, C.; Xie, J. Synergetics: The cooperative phenomenon in multi-compressions S-CO2 power cycles. *Energy Convers. Manag. X* **2020**, *7*, 100042, doi:10.1016/j.ecmx.2020.100042.
42. Turchi, C.S.; Ma, Z.; Neises, T.; Wagner, M. Thermodynamic Study of Advanced Supercritical Carbon Dioxide Power Cycles for High Performance Concentrating Solar Power Systems. **2020**, 1–9.
43. Besarati, S.M.; Goswami, D.Y. Analysis of advanced supercritical carbon dioxide power cycles with a bottoming cycle for concentrating solar power applications. *ASME Int. Mech. Eng. Congr. Expo. Proc.* **2013**, *6 A*, 2–8, doi:10.1115/IMECE2013-63753.
44. Neises, T.; Turchi, C. A comparison of supercritical carbon dioxide power cycle configurations with an emphasis on CSP applications. *Energy Procedia* **2014**, *49*, 1187–1196, doi:10.1016/j.egypro.2014.03.128.
45. Kulhánek, M.; Dostál, V. Supercritical CO 2 Power Cycle Symposium Thermodynamic Analysis and Comparison of Supercritical Carbon Dioxide Cycles Supercritical CO 2 Power Cycle Symposium. **2011**, 2–8.
46. Olumayegun, O.; Wang, M. Dynamic modelling and control of supercritical CO 2 power cycle using waste heat from industrial processes. *Fuel* **2019**, doi:10.1016/j.fuel.2019.03.078.
47. Manente, G.; Fortuna, F.M. Supercritical CO2 power cycles for waste heat recovery: A systematic comparison between traditional and novel layouts with dual expansion. *Energy Convers. Manag.* **2019**, doi:10.1016/j.enconman.2019.111777.
48. Cabeza, L.F.; de Gracia, A.; Fernández, A.I.; Farid, M.M. Supercritical CO2 as heat transfer fluid: A review. *Appl. Therm. Eng.* 2017.
49. Strzalka, R.; Erhart, T.G.; Eicker, U. Analysis and optimization of a cogeneration system based on biomass combustion. *Appl. Therm. Eng.* **2013**, *50*, 1418–1426, doi:10.1016/j.applthermaleng.2011.12.039.
50. Stehlík, P.; Zagermann, S.; Gängler, T. Furnace integration into processes justified by detailed calculation using a simple mathematical model. *Chem. Eng. Process. Process Intensif.* **1995**, *34*, 9–23, doi:10.1016/0255-2701(94)00508-7.
51. Zarrouk, S.J.; Moon, H. Efficiency of geothermal power plants: A worldwide review. *Geothermics* **2014**, *51*, 142–153, doi:10.1016/j.geothermics.2013.11.001.